Geomechanics and Engineering, *Vol. 36, No. 6 (2024) 545-561*
https://doi.org/10.12989/gae.2024.36.6.545

Numerical study on the influence of embedment footing and vertical load on lateral load sharing in piled raft foundations

Sommart Swasdi[1a], Tanan Chub-Uppakarn*[1,2], Thanakorn Chompoorat[3b] and Worathep Sae-Long[3c]

[1]*Department of Civil Engineering and Environment, Faculty of Engineering, Prince of Songkla University, Songkhla 90110, Thailand*
[2]*Southern Natural Disaster Research Center, Prince of Songkla University, Songkhla 90110, Thailand*
[3]*Department of Civil Engineering, School of Engineering, University of Phayao, Phayao 56000, Thailand*

(*Received April 25, 2023, Revised February 10, 2024, Accepted February 27, 2024*)

Abstract. Piled raft foundation has become widely used in the recent years because it can increase bearing capacity of foundation with control settlement. The design for a piled raft in terms vertical load and lateral load need to understands contribution load behavior to raft and pile in piled raft foundation system. The load-bearing behavior of the piled raft, especially concerning lateral loads, is highly complex and challenge to analyze. The complex mechanism of piled rafts can be clarified by using three dimensional (3-D) Finite Element Method (FEM). Therefore, this paper focuses on free-standing head pile group, on-ground piled raft, and embedded raft for the piled raft foundation systems. The lateral resistant of piled raft foundation was investigated in terms of relationship between vertical load, lateral load and displacement, as well as the lateral load sharing of the raft. The results show that both vertical load and raft position significantly impact the lateral load capacity of the piled raft, especially when the vertical load increases and the raft embeds into the soil. On the same condition of vertical settlement and lateral displacement, piled raft experiences a substantial demonstrates a higher capacity for lateral load sharing compared to the on-ground raft. Ultimately, regarding design considerations, the piled raft can reliably support lateral loads while exhibiting behavior within the elastic range, in which it is safe to use.

Keywords: embedded raft; finite element analysis; lateral load sharing of raft; pile group; piled raft

1. Introduction

A Piled raft foundation system is increasingly popular and has been demonstrated as a crucial system that improve stability, reduce settlement, and cost effectiveness. Previous studies have been shown that a piled raft foundation is essential for distribution of structural loads over a larger area a reducing the intensity of loads on individual points. These advantages prevent localized settlement and ensures more uniform support for the entire structure. The combination of raft and pile also helps distribute and dissipate loads, reducing the potential for differential settlement. Importantly, in an earthquake-prone area the piled raft foundation system can provide good seismic performance to enhanced of the foundation's resistance to lateral loads during an earthquake (Amornfa *et al*. 2022, Jamil *et al*. 2022, Karira *et al*. 2022a, b, Soomro *et al*. 2022). Although the piled raft foundation provides several advantages, some limitations need to be addressed such as their ability to minimize settlement in a specific soil condition that might affect stability and safety of the structure. Understanding the load-bearing behavior of a piled raft foundation, especially a lateral load resistance, is a fundamental step that guide the engineer in tailoring the foundation design to the unique construction site.

Several methods have been used to analyze a complexity of the piled raft foundation. However, the finite element method (FEM) is the most suitable approach to assessing the complexity of the piled raft system. The 3D FEM has been used in a study by Novak *et al*. (2005). It has been found to be a simple method to produce outstanding results and the FEM software is readily available, powerful, and portable. The Plaxis 3D also used to investigate the settling behavior of piled rafts to demonstrate the impacts of pile number, length, pattern and space in a study by Vu *et al*. (2014). The Ansys and Plaxis has been applied to describe the failure mechanism of the piled raft foundation (Balakumar *et al*, 2017). Watcharasawe *et al*. (2017) investigated the factors that influence the behavior of piled rafts in the Bangkok subsoil. The study used a coupled 3D mechanical and hydraulic numerical model to conduct a consolidation analysis of piled raft systems for low-rise and high-rise buildings with basement levels in clay soil, to assess the feasibility of implementing piled rafts. The load carried by piles of the piled rafts was heavily influenced by

*Corresponding author, Assistant Professor
E-mail: tanan.c@psu.ac.th
[a]Ph.D. Student
E-mail: sswasdi@hotmail.com
[b]Associate Professor
E-mail: thanakorn.ch@up.ac.th
[c]Assistant Professor
E-mail: worathep.sa@up.ac.th

ISSN: 2005-307X (Print), 2092-6219 (Online)

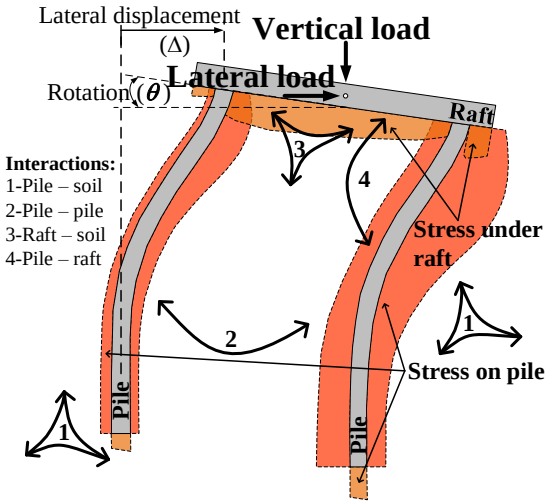

Fig. 1 Soil-structure interactions in piled raft foundation

consolidation. Azizkandi *et al*. (2018) used 1-g shaking table tests to compare the dynamic behavior of connected and disconnected piled rafts to expand on dynamic response. In addition, FEM software was utilized for numerical modeling in the laboratory and in supplementary tests. Hsueh *et al*. (2018) applied the FEM to study the interaction between piles, soil, pile cap and the consequences of concrete cracking. The result showed that the FEM create a calibrated model to represent the group's leading and middle row pile carried the highest and lowest shares of pile head loads, respectively. The 3D FEM also used to investigate the impact of alternative pile head connection conditions, namely, fixed and hinged connections, on the response of piled rafts in sand subjected to pseudo-static horizontal loading (Halder *et al*. 2020).

The finite element model was validated on geotechnical centrifuge tests by Kumar *et al*. (2016). The results showed that the rigidity of the pile head connection had a significant impact on the behavior of the piled raft in many aspects. Qin and Ma (2021) studied the seismic behaviors of pile foundations under floating-raft and embedded-raft conditions using centrifuge tests and FEM. Chanda *et al*. (2022) performed a scaled-model test on the piled raft subjected to vertical, horizontal, and moment loads to examine the lateral responses of piled raft due to the interaction of loading. The finding revealed that the vertical load significantly influences the lateral response of piled raft. A FEM model was also created and validated based on experimental data that support the prototype piled raft study. The load-sharing behavior of the prototype piled raft was also investigated using the confirmed numerical model. Jamil *et al*. (2022) performed small-scale model experiments to study the response of a basement wall in a tall buildings' foundations to lateral loading. The findings demonstrated that the demand on each pile was reduced, and the lateral displacement was decreased in the presence of a basement wall.

The piled raft represents a hybrid foundation system that amalgamates the advantages of both pile and raft foundations. The interactions among piles, the raft, and the subsoil significantly impact the bearing capacity and deformation behavior of piled rafts. In order to ensure an effective and secure design for piled rafts, it is imperative for the study to meticulously account for these interactions, as emphasized in the work by Katzenbach and Leppla (2015). The total load, encompassing vertical and lateral forces, is channeled into the subsoil through contact pressure beneath the raft and piles, facilitated by the inherent stiffness of the raft. The comprehensive resistance of the piled raft encompasses the contributions of both the raft and the piles. The resistance of the piles is influenced by factors such as base resistance, lateral bearing, and skin friction. Visualized in Fig. 1 are the interactions between the piled raft and the soil. The interplay of various components within the piled raft foundation significantly influences both the bearing capacity and the load-settlement behavior.

Examining the load-bearing characteristics of piled rafts using conventional theoretical methods has been indicated to be an intricate and challenging method. Moreover, these approaches need to capture the authentic behavior of piled rafts, particularly when considering the intricate effects of interactions on the bearing capacity. Therefore, to investigate the piled raft foundation system in a real-world practice, the application of FEM is deemed to be the most suitable approach to demonstrate the intricate and multifaceted behavior of piled raft foundations. The content of this work is drawn as follows: First, finite elements, materials, and model verification are introduced. Next, the behavior of a piled raft when subjected to lateral load while altering the vertical force and raft position is discussed based on the results of the finite element model. Finally, the observations of this work are summarized in the last section.

The effects of vertical load on-ground raft placement pattern (PR_OG), embedded raft (PR_EM) on lateral load behavior, and lateral load sharing for each pile and raft compartment in a piled raft foundation system is a crucial issue that need to be investigated in order to understand the load-baring behavior of the piled raft system. Study by

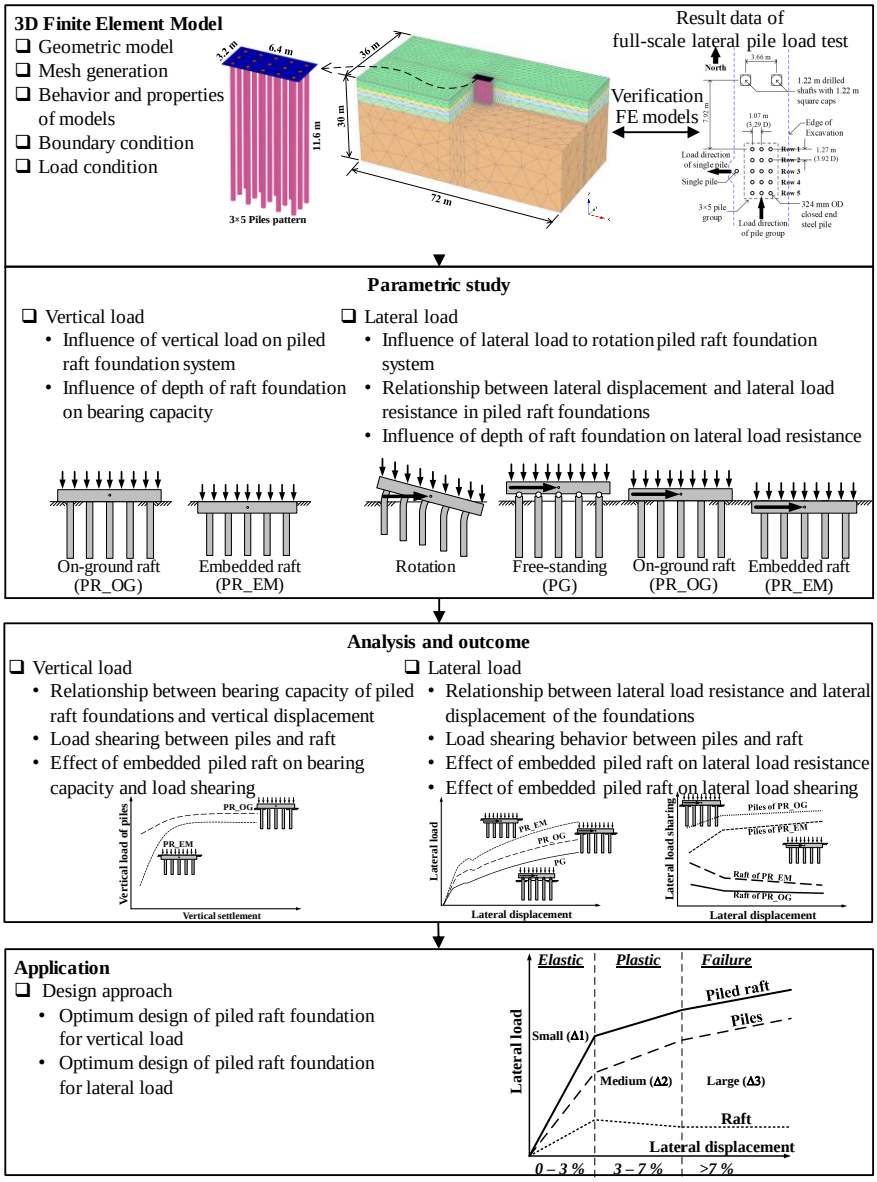

Fig. 2 Methodological framework

Jeffrey L. Snyder (Snyder 2004) use the full-scale test (FST) to investigate the behavior of the lateral piles. The piles were embedded in soft clay and silts of 11.60 m depth. The single free-standing pile and 3×5 configuration of the free-standing head pile group were used to study the behavior when subjected to lateral load. In the free-standing pile group (without raft) model, Snyder's full-scale test was utilized to investigate the lateral load behavior of a single pile and a pile group.

Currently, the investigation of the effect of rafts on lateral load uptake is limited. Therefore, this study aims to investigate the lateral load behavior in lateral load of piled rafts and load sharing of rafts by using the FEM. The influence of vertical loads, raft placement (PR_OG and PR_EM), and lateral displacement of the piled raft on lateral load behavior and load-sharing of the raft were investigated using previously unstudied areas of Snyder's FST. Vertical and lateral load deformation, piled raft rotation, vertical and lateral load sharing of piles and rafts, and piles' vertical and lateral load behavior in each row were all assessed.

2. Methodological framework

To comprehend the holistic effects of vertical load, lateral load, and raft foundation depth on a piled raft foundation system, this study employs a rigorous exploration through 3D simulation, as delineated by the methodological framework in Fig. 2. This framework guides the investigation of the lateral load capacity and load-sharing dynamics between piles and the raft foundation within the piled raft foundation system.

The initial step involves the validation of material parameters (soil, raft, and pile), along with the boundary and stress-strain behavior of the Finite Element (FE) model.

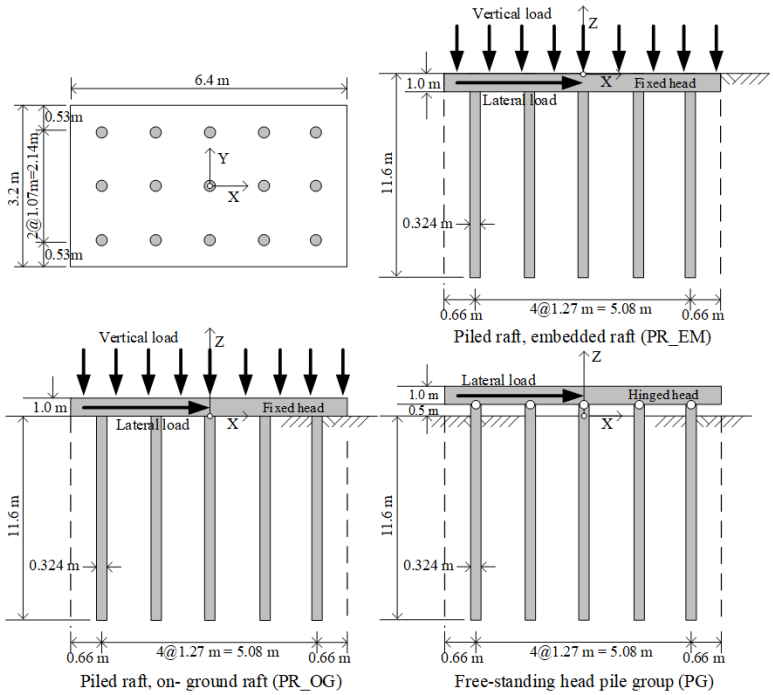

Fig. 3 Types and configurations of foundations in FE analyses

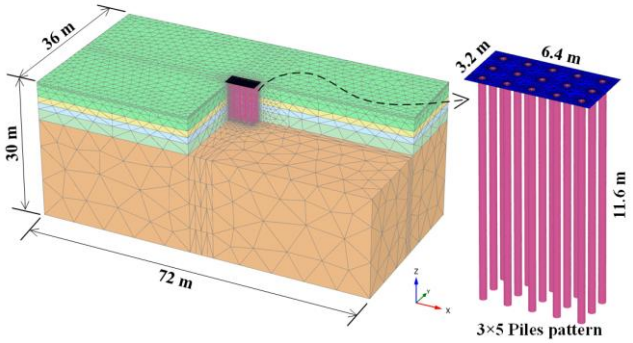

Fig. 4 Finite element model for piled rafts and pile group

This validation process closely aligns with the full-scale testing of a free-standing group pile with a free head. Subsequently, the study delves into the application of controlled vertical loading to examine the raft behavior of the piled raft foundation system. This phase aims to elucidate the intricate relationships among vertical load, vertical settlement, and load sharing between piles and the raft.

After the vertical load analysis, lateral load is systematically applied to the piled raft foundation system. This step is crucial for clarifying the complex behavior arising from the interaction of all load combinations. Leveraging the capabilities of the 3D Finite Element Model (FEM), the study aims to achieve a nuanced understanding of the piled raft foundation system's behavior under the combined influence of vertical and lateral loads and the effects of on-ground and embedded raft positions.

In conclusion, the analysis data derived from this comprehensive study will serve as a valuable resource for determining the optimal zone for both vertical and lateral loads within the design criteria. This research contributes to a broader understanding of piled raft foundation systems and provides insights that can inform more effective and resilient engineering practices.

3. Finite elements, materials, and model verification

3.1 Finite elements models

Three dimensional finite element (FE) models in this study were developed in PLAXIS 3D for all piled rafts configurations: embedded piled raft, on ground piled raft, and free-standing head pile group. The three dimensional FE models have similar characteristics of soil layers and piles but different in raft condition only as shown in Fig. 3. The FE models represented full of foundation geometry to study behavior of each pile row. The dimension of FE models is 36 m width (11.25 times of raft foundation width), 72 m length and 30 m depth (2.6 times of pile length),

Table 1 Validated soil parameters of the HSsmall model used in FEM

Parameter	Layer 1	Layer 2	Layer 3	Layer 4	Layer 5
	Silt & Clay	Sand	Silt & Clay	Sand	Silt & Clay
Depth of soil layer [m]	0-3.1	3.1-4.5	4.5-5.9	5.9-8.3	8.3-30
Unsaturated unit wt., γ_{unsat} [kN/m^3]	17	17	17.5	16.5	18
Saturated unit wt., γ_{sat} [kN/m^3]	19	19	19.5	18.5	20
Cohesion, c'[kN/m^2]	15	0	16.92	0	30.45
Friction angle, φ'[°]	25	38	26	33	28
Secant stiffness in drained triaxial, E_{50}^{ref} [kN/m^2]	2×10^4	4.2×10^4	2.26×10^4	3.65×10^4	4.06×10^4
Tangent stiffness for primary oedometer loading, E_{oed}^{ref}[kN/m^2]	2.56×10^4	5.04×10^4	2.89×10^4	4.38×10^4	5.2×10^4
Unloading/reloading stiffness, drained triaxial, E_{ur}^{ref} [kN/m^2]	9.48×10^4	1.54×10^5	1.07×10^5	1.34×10^5	1.93×10^5
Reference shear modulus at very small strains, G_0^{ref} [kN/m^2]	2.7×10^5	1.4×10^5	3.05×10^5	1.22×10^5	5.49×10^5
Threshold shear strain at which G_s=0.722G_0, $\gamma_{-0.7}$ [-]	1.2×10^{-4}	1.5×10^{-4}	1.25×10^{-4}	1.75×10^{-4}	1.5×10^{-3}

which is sufficient size to diminish the boundary effect. Bottom boundary of the model is fixed in all directions but side boundaries were given a horizontally constrained condition. In order to improve computation efficiency and reduce time consumption, the soil element surrounding piles and raft need to finer meshes and soil element size increases gradually in direction away from the piled raft foundation structure. The geometry and mesh dimensions for the FE models are shown in Fig. 4. The pile was defined as an embedded beam in Plaxis 3D, consisting of beam elements with embedded interface elements to describe the interaction with the soil at the pile skin and the pile tip (end bearing capacity). The interaction of the pile with the soil at the skin of the pile was described by linear elastic behavior with a finite strength. Interface elements were used between the soil and foundation components of piled rafts, with the interface shear strength being 67 percent of the soil strength (D'Aguiar *et al*. 2008, Knappett and Craig 2019, Tomlinson & Woodward 2007). The connection between the piles and the raft was decided to be a fixed-head condition except free-standing head pile to be pin condition.

3.2 Material constitutive models

The piles raft foundation under vertical load and horizontal load is a nonlinear problem because of the nonlinear material behavior of piles, raft foundation and soil and due to gap formation at the pile-soil interface. In this study, the nonlinear behavior of soil material is accounted for using hardening soil with small strain (HS-small) model and the pile elements were defined as elastoplastic constitutive model.

3.2.1 Soil model

The hardening soil (HS) model assumes elastic material behavior during unloading and reloading. The strain range in which soils can be regarded as really elastic, where they recover almost fully from applied strain, is relatively small. Soil stiffness decreases nonlinearly as strain amplitude increases. The material's high stiffness at low strain levels ($<10^{-5}$) is one soil behavior element still missing from the HS model. Small-strain stiffness can play a significant role even in applications where engineering strain levels ($>10^{-3}$) are dominant. It is widely acknowledged that traditional models overestimate heave in excavation difficulties. These HS models also overestimate the width of the settlement trough behind excavations and above tunnels while underestimating the gradient. This can be improved by small-strain stiffness. In addition, small-strain stiffness can be employed in applications involving cyclic loading and dynamic behavior to model the influence of hysteresis and hysteretic damping (Plaxis 2020). The HS-small model's advanced characteristics are most noticeable in working load conditions. The HS-small provides more accurate displacements than the HS model in this case. The HS-small model introduces hysteretic material dampening when employed in dynamic applications. As a result, this advanced constitutive model is well-suited for static and dynamic analysis. The HS-small model, which is included in Plaxis 3D, was used to define all soil models. The next section shows the outcomes of the analysis with the above settings. Field test results and FEA results for analyzing the lateral load behavior of a single free-standing pile and pile group are consistent and similar.

The validated parameters for each soil layer used in the FEA are listed in Table 1. The dilatancy angle (ψ) is 0°, tension cut-off and tensile strength (σ_t) is 0 kN/m^2, power for the stress-level dependency of stiffness (m) is 0.5, Poisson's ratio for unloading-reloading (ν_{ur}) is 0.2, failure ratio (R_f) is 0.9, the interface reduction factor (R_{inter}) is 0.67, and the analysis type of all soil layers is drained type. Snyder's field test data were utilized to calibrate the

Table 2 Parameters of piles and rafts for FE model

Parameters of piles		Parameters of rafts	
Outside diameter of steel tube pile, D_p [m]	0.324	The thickness of the raft, t_r [m]	1.00
Wall thickness of steel tube pile, t_p [mm]	9.5	Raft size, $Br \times Lr$ [m^2]	3.2×6.4
Structure behavior	3D Embedded beam	Structure behavior	3D Plate
Material type	Elastoplastic	Material type	Elastoplastic
Elastic modulus, E [kN/m^2]	200×10^6	Elastic modulus, E [kN/m^2]	23×10^6
Max. normal force, N_p [kN]	3141	Max. normal force, N_p [kN/m]	5485
Max. bending moment, M_p [kN m]	350	Max. bending moment, M_p [kN m/m]	1583

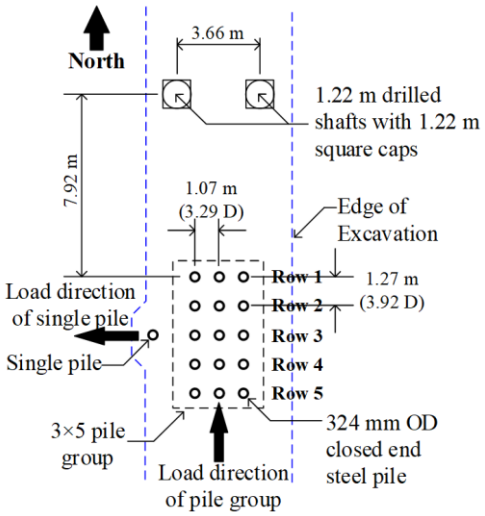

Fig. 5 The layouts of single pile and 15-pile group in 3×5 configuration of Snyder's full-scale test (Snyder 2004)

parameters for the FEA. The soil layer data in the field were converted into various parameters of the HSsmall soil model based on the results of past studies (Likitlersuang *et al*. 2018, Likitlersuang *et al*. 2013a, Likitlersuang *et al*. 2013b, Surarak 2010, Vakili *et al*. 2013, Watcharasawe *et al*. 2017, Zhao *et al*. 2015). All of the soil parameters used for finite element analysis have been validated. As demonstrated in the following section, using the validated parameters in the finite element model can yield analytical findings that are reliable and comparable to the outcomes of field tests.

3.2.2 Pile and raft model

The FE model parameters define the behavior of the piles as 3D embedded beams with elastoplastic material type. The yield bending moment of a steel tube pile is 350 kN-m, and it employs the same engineering parameters as in-field testing. However, to reduce the influence of the resistance force at the pile tip caused by the different levels of the pile tip, pile ends of the free-standing head pile group (PG), on-ground piled raft (PR_OG), and embedded piled raft (PR_EM) patterns are at the same level.

For the attachment of the heads of piles to the raft, in the case of the single free-standing pile and free-standing pile group, these were defined as hinge connections or as fixed connections for the piled raft foundation. Concrete with a thickness of 1.00 m and a size of 3.2 m×6.4 m defined the raft. The raft was modeled as a 3D plate with elastoplastic material type. Table 2 shows the engineering properties of piles and raft.

3.3 Validated parameters of soils, piles, and raft and verification of FE model

The FE model in this study was validated using a full-scale lateral load test (FST) in the single pile (SP) and pile group field, reported by Jeffrey L. Snyder. Free-standing head pile group (PG) was embedded in soft clay and silt layers at Salt Lake City International Airport, Utah, the USA, using tube-steel piles with diameter (Dp) 324 mm, and thickness 9.5 mm. Specifications of the steel piles are ASTM 252 Grade 3 with an average yield strength of 404,592 kPa, and an average tensile strength of 584,087 kPa. In addition, the steel piles have a yield moment of 350 kN-m. Piles were embedded into the soil to 11.6 m, and the head of the piles protruded from the soil surface for approximately 2.1 m. The distance between the piles was

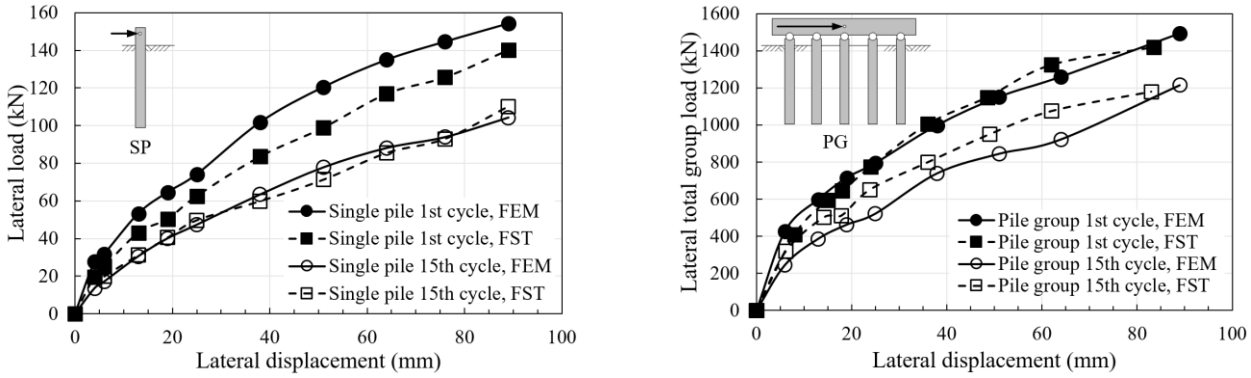

(a) Single pile (b) Pile Group

Fig. 6 Lateral load-deflection of FST and FEM for 1st and 15th cycle lateral load

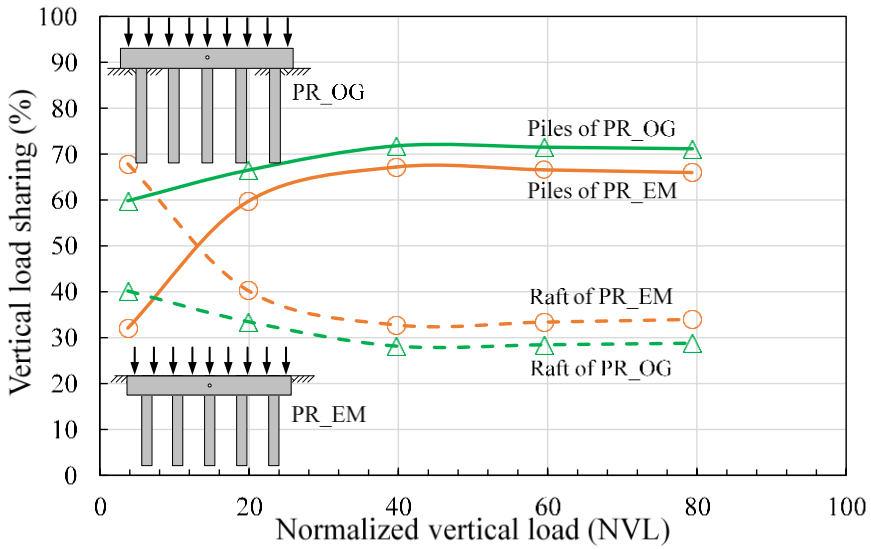

Fig. 7 Vertical load shares of piles and raft versus normalized vertical load of PR_OG and PR_EM

1.27 m (3.92D) in the direction of 5 piles and 1.07 m (3.29D) orthogonally for 3 piles. The strain gages were installed along the length of the pile to measure strain during testing, and a single pile and pile groups in 3×5 configuration were tested. For the pile group, loads were applied parallel to the direction of 5 piles (Fig. 5). Two 1.34 MN (150 ton) hydraulic jacks were used to apply a static lateral force during the test. For single pile testing, the pile head had to move laterally for a defined distance of 6 to 90 mm, and for pile group testing, the pile heads had to move laterally for a distance of 13 to 90 mm. The force was repeated 15 times for each specified lateral movement distance, during which the lateral movement and lateral load readings were recorded. And, in each cycle of the test, the load was exerted until the desired distance had been reached, then held for 5 minutes, then released to zero, and then gradually raised in the following cycle until 15 cycles have been completed. The test results are presented after this.

Using the geotechnical engineering software Plaxis 3D, the test results of lateral load behavior FST of single pile and pile group were compared with FEM. Plaxis 3D utilized an elastoplastic 3D embedded beam model for piles and a HSsmall model for soil. Snyder's FST data were used in the FEA for the soil and pile data. All soil parameters were verified before use in the final analysis. As a result, the FST results and the FEA had a consistent and close relationship.

The analysis results are consistent and similar to the effects of field testing after the FE model has been validated. When considering the foundation as a piled raft, the above model was used to examine the lateral load behavior of the pile group, considering that the raft helps absorb the loads operating on the foundation. A FE model of this type was utilized in analyzing the lateral load behavior of the piled raft for influences of vertical load and raft positioning in additional analysis expanding from Snyder's FST, such that has not been studied before.

The relationship between lateral load and lateral deflection of Snyder's FST and FEM for each lateral displacement, from the tests and from the simulations, for load cycles 1 and 15, are shown in Fig. 6. Between field testing and FEA based on soil and pile parameters identified from field testing, the lateral load-displacement behaviors

Table 3 The piled rafts' reactions to different vertical load magnitudes

Type of piled raft	Vertical load [kN] (V)	Vertical settlement of piled rafts [%] (δ_V)	Normalized vertical load (NVL) ($V/\gamma DpBrLr$)	
PR_OG	492	0.15	3.75	V1
	2602	0.80	19.85	V2
	5205	1.87	39.70	V3
	7807	5.85	59.54	V4
	10410	10.01	79.39	V5
PR_EM	492	0.14	3.75	V1
	2601	0.79	19.84	V2
	5201	1.82	39.67	V3
	7802	4.38	59.51	V4
	10403	9.28	79.34	V5

Remark: Average total unit weight of all soil layers (γ) = 19.76 kN/m^3, diameter of pile (Dp) = 0.324 m, width of raft (Br) = 3.20 m, length of raft (Lr) = 6.40 m, and vertical settlement of piled rafts given in percent of the diameter of piles

of single pile and pile groups were consistent and similar.

The behavior of soil heave in front of piles and gap formation behind piles under lateral loads can be clearly illustrated in field tests and FEA. From FST and FEM, Fig. 6(a) depicts the behavior of lateral load versus lateral displacement of a single pile. The lateral load of a single pile is slightly higher than in FST in the first cycle, in the FEM simulation. Still, when the lateral load cycle 15 is considered, the FST and FEM lateral loads are identical. The lateral load behavior of the pile group is shown in Fig. 6(b). The FST test and the FEM results were similar for the first cycle load. When the number of load cycles was increased to 15, it was discovered that the lateral load response of the pile group in the FST was slightly higher than in the FEM investigation. The lateral load behaviors of the single pile and pile groups were consistent. According to Plaxis 3D FE model study, employing soil and pile data from Snyder's FST, the study results were practically identical. As a result, the FE model will be used to investigate the behavior of the piled raft under the effect of lateral load, while varying the vertical load and raft placement, which Snyder's FST did not investigate. The study's findings are reported in the next section.

4. The behavior of a piled raft when subjected to lateral load while altering the vertical force and raft position

4.1 Influence of vertical load on vertical load sharing of PR_OG and PR_EM

To understand the load contribution patterns of rafts and piles, it is necessary to examine the impact of the vertical load magnitude operating on the piled rafts foundation system (PR_OG and PR_EM) on load shearing on rafts and piles. Table 3 represents the applied vertical load condition in the piled raft foundation. The vertical load-sharing behavior of the piles and rafts as shown in Fig. 7 directly affected the magnitude of applied vertical load and the embedded raft foundation condition. It could be seen that the mobilization of load carried in the raft and piles changed with increasing vertical load due to settlement in the piled raft foundation system. When the vertical load rose to a normalized vertical load (NVL) of roughly 40, the mobilized vertical load on the raft progressively diminished and stabilized. Conversely, the raft's position on the ground resulted in a lower vertical load capacity than for the embedded kind, and the piles developed a bigger vertical load capacity than the raft.

The vertical load sharing of piles increased significantly with load (from 60% to 72%) for PR_OG in the normalized vertical load (NVL) smaller than the 39.70 range (vertical settlement of piled raft (δ_V) less than 1.87% of pile diameter). When NVL exceeded 39.70 (δ_V > 1.87%), the vertical load shearing stabilized at 72%. On another hand, In the PR_EM configuration, as NVL ranges from 3.75 to 39.67 (δ_V = 0.14 – 1.82%), there is an observed increase in the distribution proportions of pile shares with respect to vertical load, rising from 32% to 67%. Upon exceeding an NVL threshold of 39.67 (δ_V > 1.82%), the proportions of pile shares remain constant at 67%. The variation in the behavior of both piled raft foundation configurations can be attributed to the influence of overburden pressure exerted on the surrounding soil as shown in Fig. 7.

In the PR_OM configuration, the vertical share of the raft experienced a decrement from 40% to 28% in response to vertical loading, with stabilization occurring at the 28% mark as the NVL exceeds 39.70. However, the performance of PR_EM pattern piled raft foundations was significantly influenced by the overburden pressure exerted by the surrounding soil. Specifically, the vertical load share of the raft exhibited a notable reduction from 68% to 32% within the range of NVL between 3.75 and 39.67. Subsequently, as the NVL exceeded 39.67, the vertical load share stabilized at 32%.

The analysis results reveal a significant degradation in raft shearing within the embedded raft (PR_EM) configuration and a corresponding increase in pile shearing compared to the on-ground raft (PR_OG) configuration, particularly when the settlement of the piled raft foundation is less than 1.8% of the pile diameter. However, once the displacement of the foundation exceeds 1.8% of the pile diameter, the shearing behavior of both raft and piles in both patterns remains relatively constant. The raft within the PR_EM pattern exhibited a vertical load shearing of 32%, which surpasses the corresponding shearing value observed in the PR_OG pattern, which stood at 28%. Conversely, in terms of pile shearing, the PR_EM pattern recorded a value of 67%, whereas the PR_OG pattern registered a slightly higher value of 72% as shown in Fig. 7.

In order to comprehend the load shearing behavior of

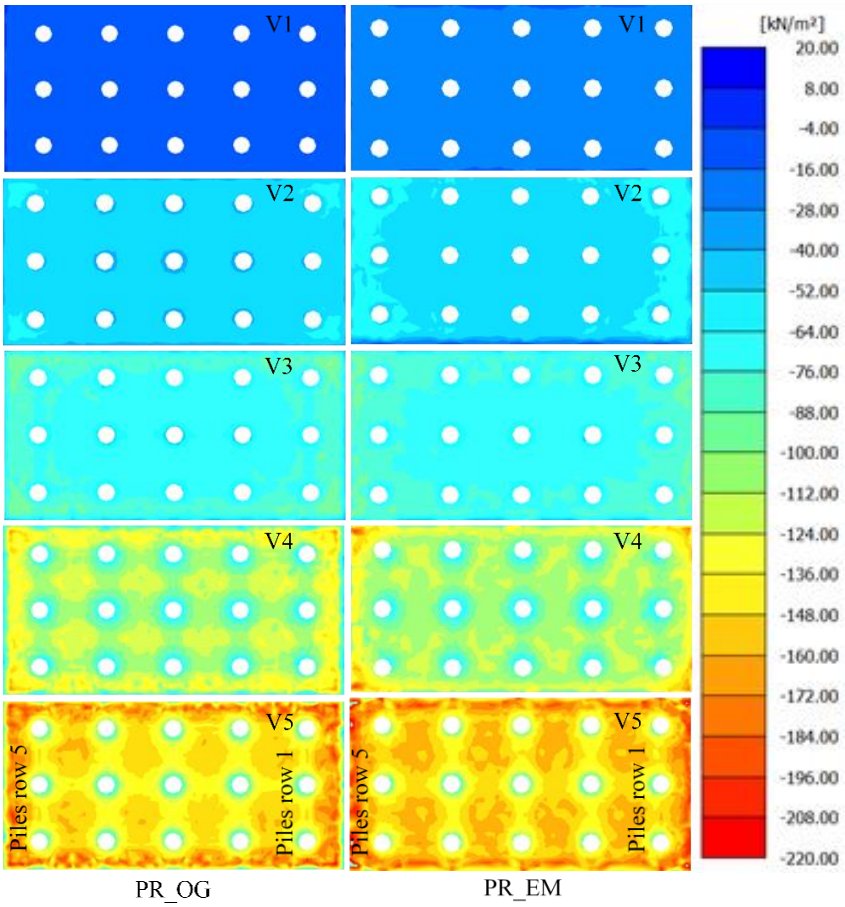

Fig. 8 Vertical stress in soil mass beneath raft at the various vertical loads, for PR_OG and PR_EM

piles and raft in piled raft foundations, it is imperative to investigate the vertical stress distribution within the soil mass beneath both piled raft patterns. Fig. 8 illustrates the vertical stress distribution beneath the rafts of both PR_OG and PR_EM types as the vertical load varies. The investigation reveals that as the vertical load escalates, the vertical stress exerted on the soil beneath the raft proportionately increases. Initially, this increase in vertical stress is observed across all edges of the raft, extending gradually towards the central region of the raft. Once the stress increment encompasses the entire perimeter of the raft, the load shearing behavior of the piled raft foundation stabilizes at a constant level. At equivalent NVL levels, the vertical stress exerted on the soil beneath the PR_EM type raft exceeded that of PR_OG. Consequently, the PR_EM type raft exhibited greater capability in sharing vertical loads compared to the PR_OG type raft. The factor influencing the vertical load carrying of the raft was its placement, particularly when the raft was embedded in the soil.

4.2 Rotation of piled raft under lateral loading with various vertical loads

The investigation into the lateral load response of the piled raft discovered that as the lateral load is applied to the piled raft, it shifts in the direction of the force. This behavior induces subsidence and rotation of the piled raft, leading to uneven distribution of vertical and lateral loads among the piles in each row. Schematically depicted in Fig. 9(a), the rotational characteristics of the piled raft under both vertical and lateral loads.

Fig. 9(b) shows the different deformation pattern of piled raft (PR) and free-standing head pile group (PG) under vertical and lateral loads. In piled rafts, the piles and rafts were connected firmly, whereas in free-standing head pile groups, hinge connections were utilized. PR exhibited an increase in the angle of rotation of the raft as the lateral displacement increased. In contrast, for PG, there was no change in the rotation angle of the raft with lateral displacement. Furthermore, the attachment pattern of the pile head and the raft in PR and PG types led to distinct lateral displacement responses of these piles, as shown in Fig. 9(b).

Fig. 10 shows the rotation angles of PR_OG, PR_EM and PG with variations in lateral displacement and vertical load. The results showed that the rotation angle of both PR_OG and PR_EM increased with lateral displacement. In terms of the influence of raft orientation on on-ground (PR_OG) and embedded (PR_EM) rafts, the results showed that the angle of rotation of PR_EM was 22.3 percent lower than that of PR_OG at a 10 percent lateral displacement. In terms of the influence of vertical load on the angle of rotation of a piled raft, it was observed that at the same

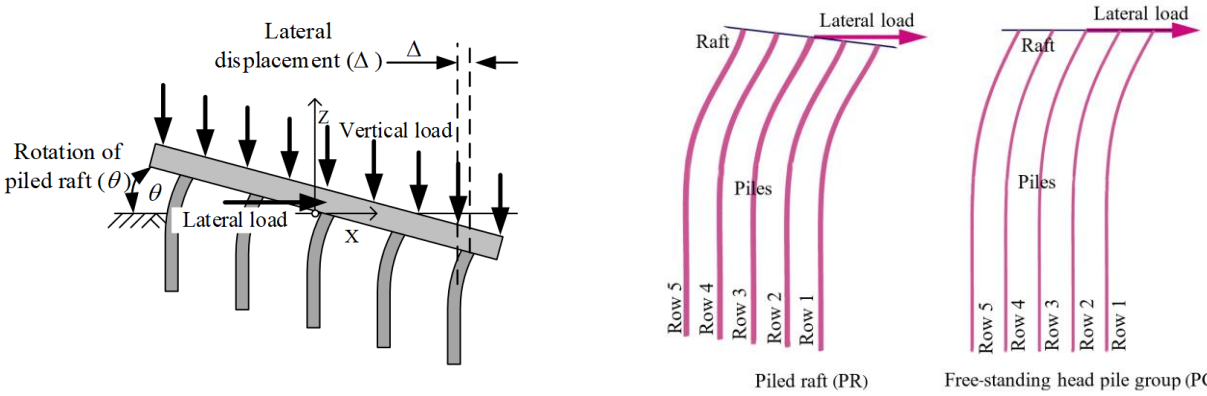

(a) Schematic of rotation of piled raft under vertical and lateral loading

(b) Deformation pattern under the acting of lateral loading

Fig. 9 Schematic of rotation and deformation of piled raft under lateral loading

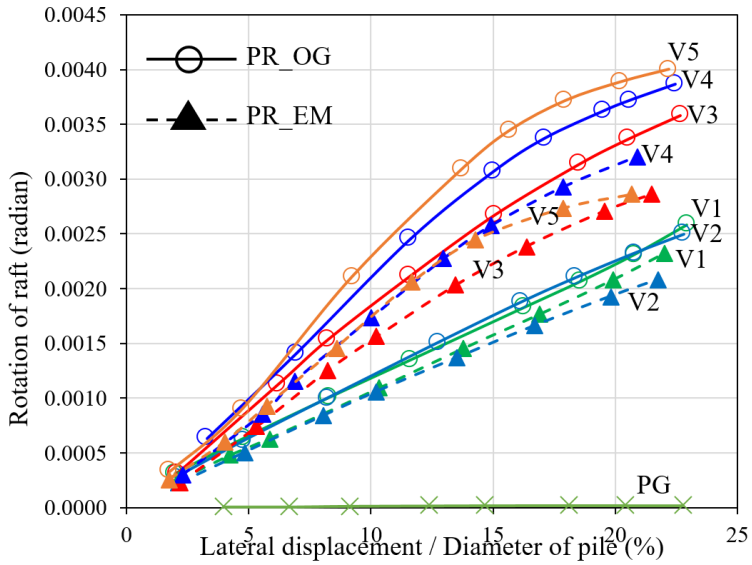

Fig. 10 Rotation of piled raft versus lateral displacement of PR_OG and PR_EM at various vertical loads

lateral displacement, the angle of rotation remained relatively consistent when NVL ranged from 3.75 to 19.85 (V1-V2). However, it increased as NVL escalated within the range of 39.70 to 79.39 (V3-V5) for both PR_OG and PR_EM. The angle of rotation increased with NVL due to the piled raft's heightened lateral load capacity as the vertical load escalated, as demonstrated in the subsequent section. Consequently, as a result of the hinge connection between the piles and the raft, which prevented the raft from rotating after bearing lateral loads, the rotation angle of PG approached zero. The rotation angle did not change as the lateral displacement increased. According to the study's findings, embedding the raft in the soil could minimize the angle of rotation of the piled raft.

4.3 A change in the vertical load influences the vertical load sharing of piles in a piled raft under lateral load

The result demonstrated that while PR_OG and PR_EM were subjected to lateral loads, the piled raft moved in the direction of the load, resulting in subsidence and rotation of the piled raft, as mentioned above. Consequently, the vertical and horizontal load-bearing behavior of the piles in each row differed. The difference in the vertical loading of the piles in each row was considered when the piled raft was subjected to lateral loads, weighing the influence of vertical loads.

Fig. 11 shows the relationship between the average vertical load occurring in each pile row of PR_OG and PR_EM. During the small vertical load action (NVL = 3.75, V1), pile rows 3, 4, and 5 varied from compressive to tensile loads. The tensile loads increased as the piled raft experienced more lateral displacement. In pile rows 1 and 2, the compressive load increased with lateral displacement. Additionally, as the vertical load increased (NVL ≥ 39.70, V3), the average vertical load occurring in all pile rows became compressive, with no tension in the piles. Conversely, pile rows 4 and 5 exhibited a progressive decrease in compression. This trend remained consistent between PR_OG and PR_EM. The results showed that when a sufficient vertical load (NVL ≥ 39.70, V3) was

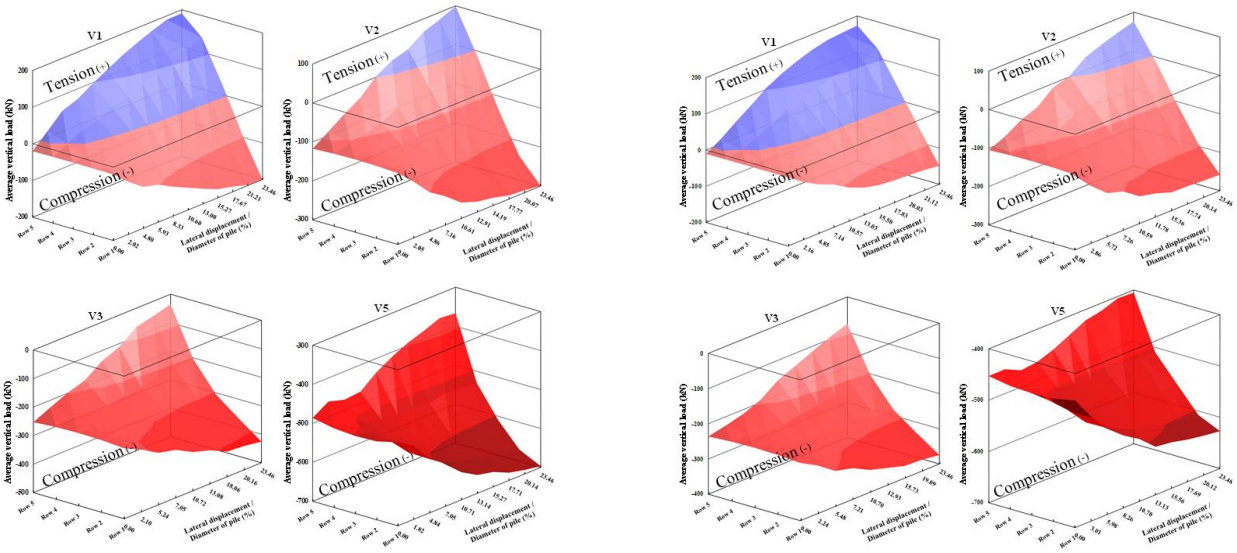

(a) PR_OG ((b) PR_EM

Fig. 11 Average vertical load of piles versus lateral displacement

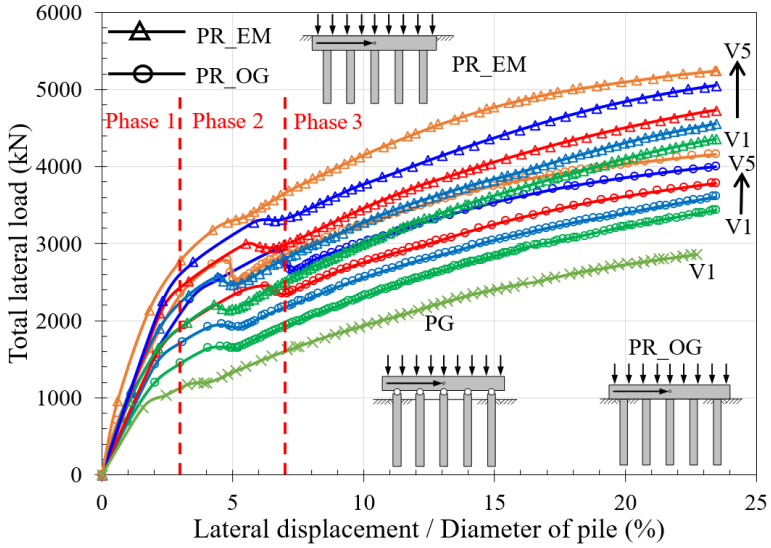

Fig. 12 Total lateral load versus lateral displacement for PR_OG, PR_EM and PG, labeled by the various vertical loads

applied to the piled raft, tensile forces were not generated in the piles in response to lateral loading.

4.4 Piled raft behaviors under lateral load for various vertical loads

The lateral load capacity of PG, PR_OG, and PR_EM based on FEM analysis, for studying the effects of vertical load on lateral loading response, are shown in Figs. 12-13. The PG exhibited a lower lateral load capacity compared to PR_OG and PR_EM at similar vertical loads. The lateral load capacities of PR_OG and PR_EM were found to be 19 and 54 percent higher than that of PG at 10 percent lateral displacement. Due to the influence of the raft, the pattern of fixing the pile heads with the raft and a vertical load of PR_OG and PR_EM allows these foundations to have an increased lateral load capacity compared to PG without the raft. The lateral load capacities of PR_OG and PR_EM improved as the vertical load increased. At 10 percent lateral displacement, the average lateral load capacity of PR_EM was 29 percent higher than that of PR_OG, attributed to the influence of the raft placement in PR_EM, which is embedded in the soil. Therefore, the lateral load performance of PR_EM is increased compared to PR_OG.

In Figs. 12 and 13, the curves were not smooth in Phase 2 because Phase 2 represented a plastic zone. In this zone, all the curves showed a transition to decreasing load-bearing capacity of the structure and soil. This indicated the yield point of the soil and the structure, typically occurring after the elastic zone (Phase 1), resulting in a decrease in load capacity and leading to a non-smooth graph. This behavior was also evident in the curve of the full-scale test (FST) as shown in Fig. 6(b) (Pile group 15th cycle, FST).

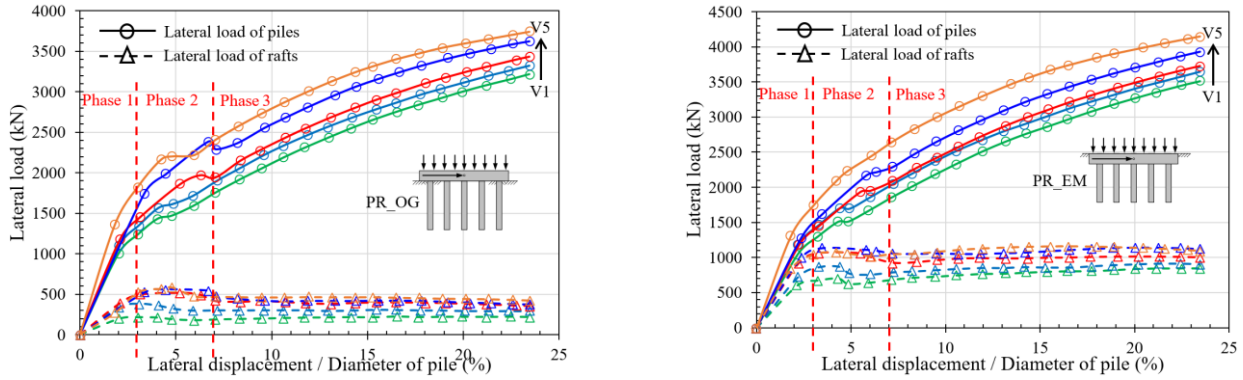

(a) PR_OG ((b) PR_EM

Fig. 13 Lateral load versus lateral displacement of piles and raft labeled by the various vertical loads

Considering the lateral loads of the piles and the rafts separately (Fig. 13), it was observed that the lateral load of the piles behaved similarly to the lateral load of the pile group of FST in Fig. 6(b). The lateral load of the rafts in Phase 2 also exhibited yielding in the plastic zone.

Fig. 13(a) shows the relationship between lateral loads and lateral displacement for PR_OG, separately considering the lateral loads of piles and raft. It was found that the lateral load of the raft increased significantly over the 0 – 5% lateral displacement range, then decreased and remained relatively stable when the lateral displacement was greater than 7% for NVL = 3.75 – 79.39 (V1 - V5). Fig. 13(b) shows the lateral load behavior of PR_EM. Considering the lateral load of the raft, it increased with a constant slope when the lateral displacement was 0 – 3%, and the NVL was in the range of 3.75 – 19.84 (V1 - V2). As the lateral displacement increased further, the lateral load remained relatively constant. For NVL = 39.67 – 79.34 (V3 - V5), the lateral load of the raft increased in the range of lateral displacement from 0% to 5%, then decreased slightly and stabilized at lateral displacements greater than 7%.

The lateral load of the raft of PR_EM was approximately 130% greater than that of the raft of PR_OG due to the influence of embedding the former raft. The above data showed that the lateral load-carrying capacity of the piled rafts depended on both the vertical load applied and the extent of lateral displacement. While the vertical loads were small (V1 - V2), the lateral load capacity of the raft peaked at approximately 3% lateral displacement. As the vertical load increased (V3 - V5), the raft exhibited its maximum effectiveness for lateral load at 5% lateral displacement. The lateral load decreased and began to stabilize at lateral displacements greater than 7%. Therefore, when the lateral displacement exceeded 7%, the increased lateral load capacity of the piled raft was mainly attributable to lateral loading of the piles.

Based on the analytical data obtained from the analysis of PG, PR_OG, and PR_EM, the behavioral characteristics of piled raft systems can be delineated into three distinct phases, as illustrated in Fig. 14:

- Phase 1 (Elastic zone, Fig. 14), when lateral displacement is from 0% to 3% of the pile diameter. The piled raft has the same lateral load behavior between the raft and the piles. The relationship between lateral load and displacement is linear for both rafts and piles, as shown in Fig. 13.

- Phase 2 (Plastic zone, Fig. 14), occurred when lateral displacement ranged from 3% to 7% of the pile diameter, indicating a distinct separation in load behavior between the raft and the piles in the piled raft system. The raft's lateral load capacity decreases, while the piles have a nonlinearly increasing lateral load, as shown in Fig. 13.

- Phase 3 (Failure zone, Fig. 14), occurring when the lateral displacement exceeded 7%, resulted in almost all of the increase in piled raft lateral load being distributed to the piles. The lateral load increased in a nonlinear fashion with lateral displacement. In this phase, the lateral load of the raft remained relatively stable when the displacement exceeded 7% of the pile diameter.

The aforementioned lateral load behavior was consistent across PR_OG and PR_EM. This behavior aligns with the findings of Shirato (2009), whose study determined that the elastic limit of lateral displacement for the pile group falls between 4% and 6% of the pile diameter. It was found that the design threshold displacement at ground level was approximately 2% to 4% of the pile diameter for the serviceability limit.

The relationship between the mean lateral load and lateral displacement of piles within each row under varying vertical loads of PR_OG and PR_EM configurations is shown in Fig.15. The results indicated that the piles in each row exhibited similar lateral loads for both PR_OG and PR_EM at lateral displacements of 2 – 3%. This behavior remained consistent when varying the vertical load, with the relationship between lateral load and lateral displacement increasing linearly during such lateral displacement. When the lateral displacement exceeded 3%, it became evident that during the small vertical load (NVL = 3.75, V1), the lateral load of the piles varied significantly by row. The first row bore the highest lateral load, followed by 2nd, 3rd, 4th, and 5th rows. The lateral load of the piles in each row increased as the vertical load increased. The results also indicated that the lateral load of the piles in the 1st row did

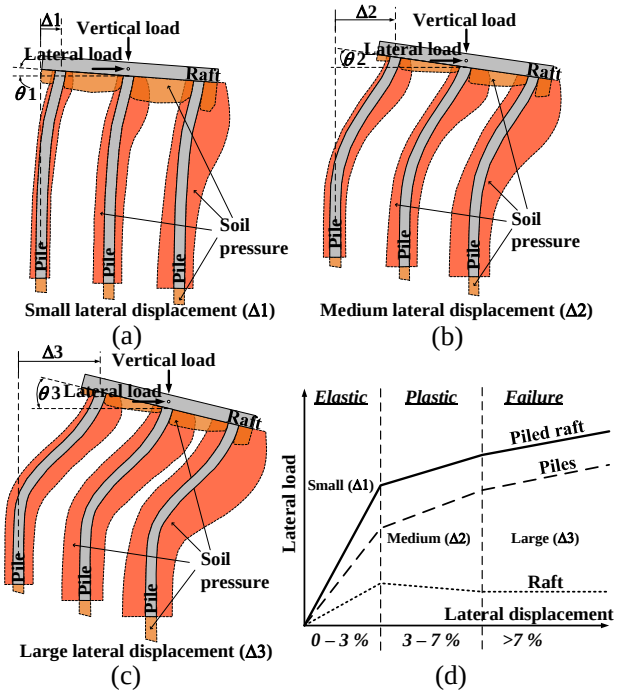

Fig. 14 Behavior under lateral loading and lateral displacement of a piled raft

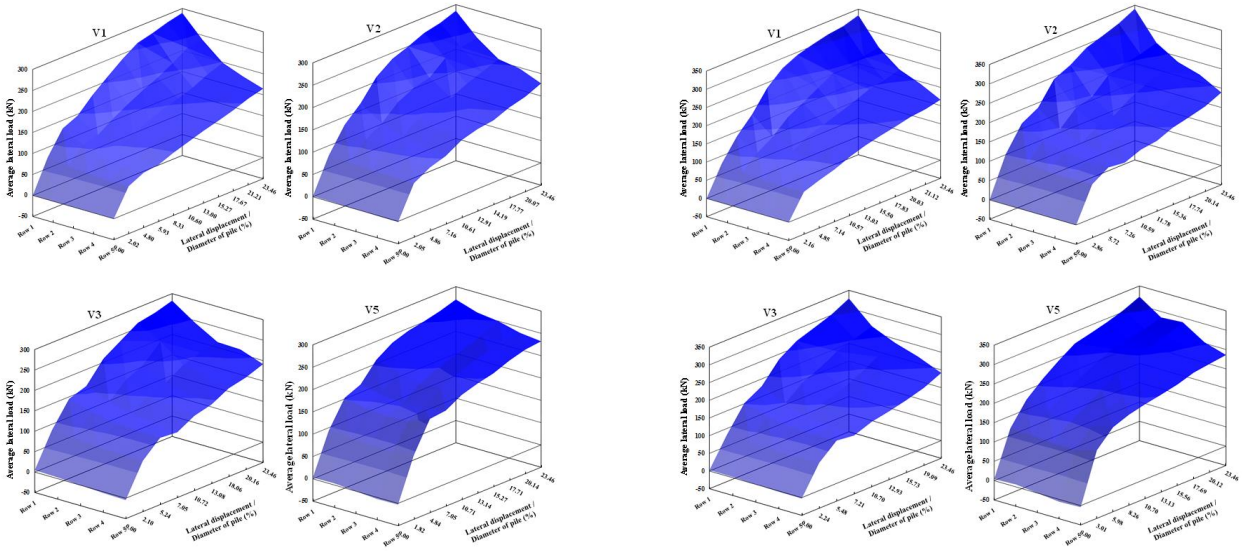

(a) PR_OG (b) PR_EM

Fig. 15 Average lateral load of piles versus lateral displacement

not change significantly compared to the other rows with the variation in vertical load. Fig. 15 also illustrated that the lateral load for PR_EM was significantly higher than for PR_OG, attributable to the influence of the embedded raft position.

The piles in the first row, situated at the front row of the piled raft, exhibited similar average lateral load magnitudes as the vertical load changed. In the last row of the piled raft, the average lateral load varied and tended to increase with vertical load. In the first and the last row of PR_OG and PR_EM configurations, the lateral load also increased with lateral displacement as illustrated in Fig. 16.

Fig. 16(a) and 16(b) show that when the lateral displacement exceeded 7 percent, the lateral load of the 5th-row piles tended to increase linearly and increased with the same slope as the vertical load. Based on the provided data, it was observed that increased vertical load did not affect the lateral load of the 1st-row piles; in other words, the effect remained consistent regardless of changes in the vertical load. However, vertical load influenced the lateral load of piles in the 5th-row, resulting in more lateral load with an increase in vertical load.

Fig. 17 displays the lateral stress in the soil mass beneath the raft under a lateral load, resulting in a lateral

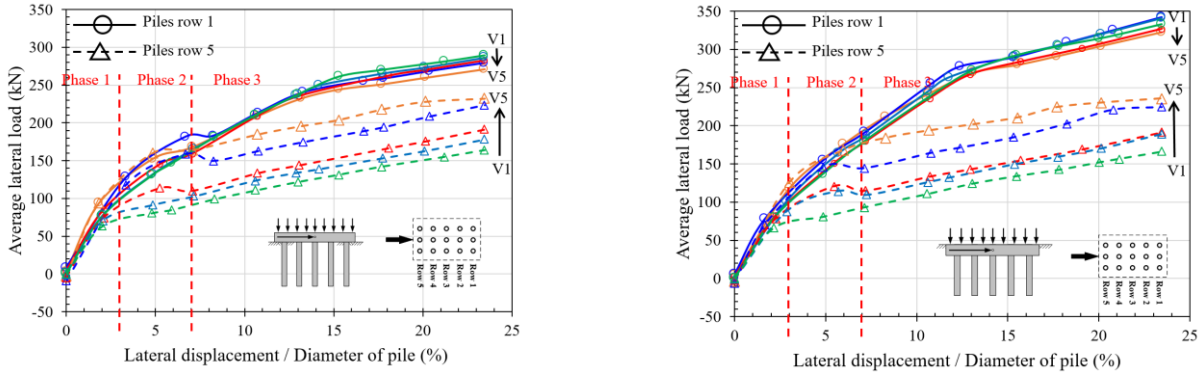

(a) PR_OG (b) PR_EM

Fig. 16 Average lateral load of piles versus lateral displacement in pile rows 1 and 5, under various vertical loads

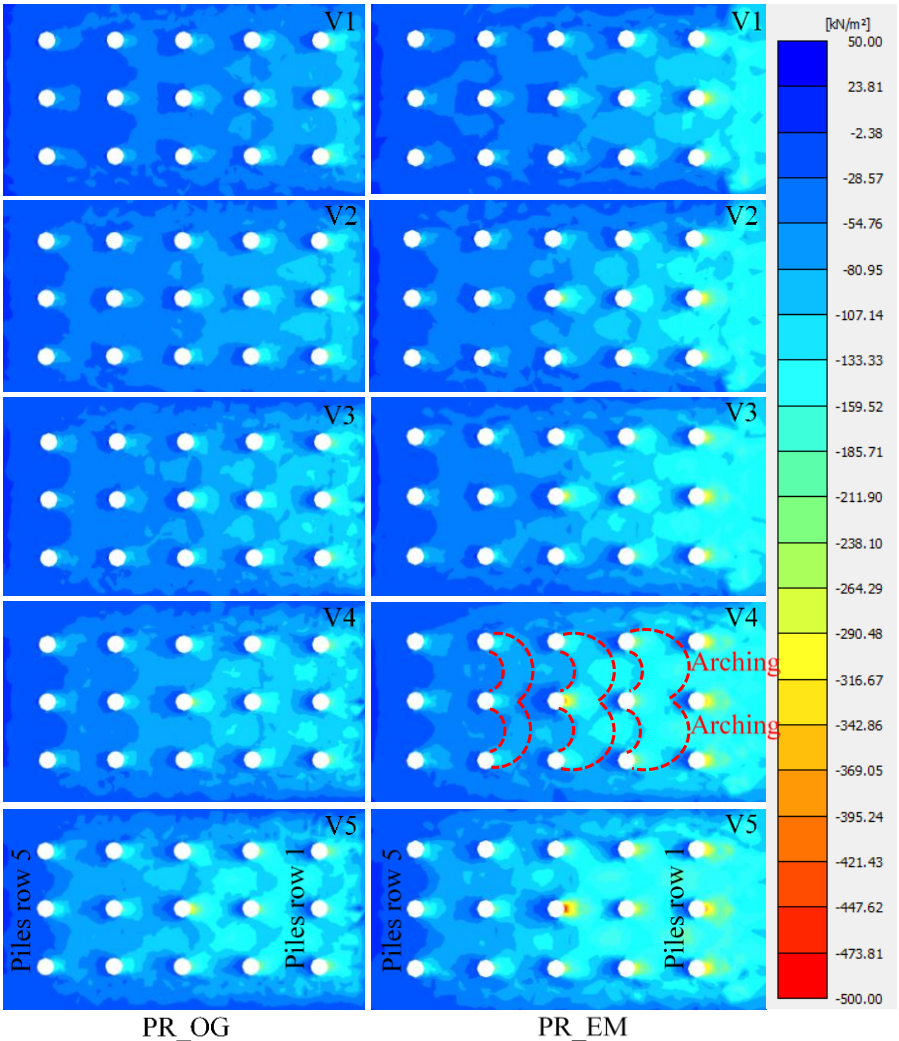

Fig. 17 Lateral stress in soil mass beneath the raft when the lateral displacement is 23.46%, for various vertical loads on PR_OG and PR_EM

displacement of 23.46 percent. This analysis was conducted using FEM and involved PR_OG and PR_EM, with vertical load being varied. The lateral stress in the soil mass on the side of lateral loading, specifically with the piles in the 1st-row, exhibited minimal variation as the vertical load increased. This consistency aligns with the lateral loads of the piles in the 1st-row, which remained unchanged when the vertical load was altered, as discussed previously. The lateral stress in the soil mass caused by the piles in the 5th-row exhibited a significant increase with vertical load. As

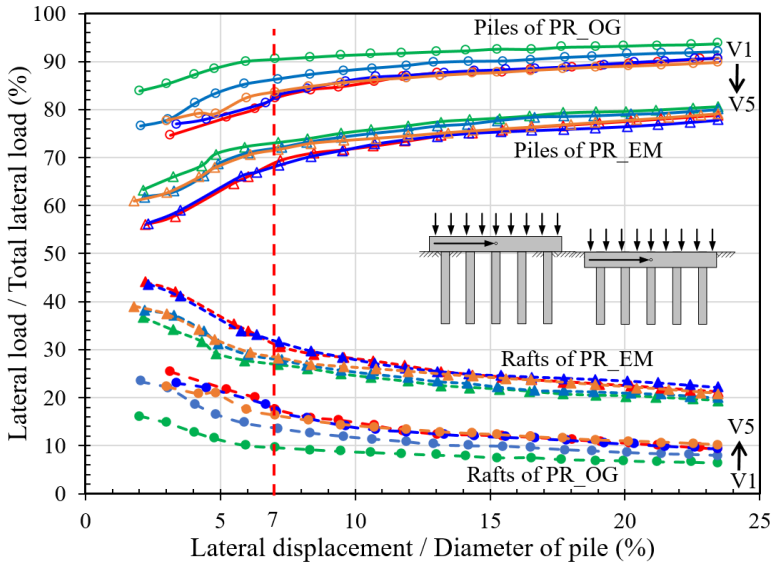

Fig. 18 Lateral load shares versus lateral displacement for PR_OG and PR_EM under various vertical loads

previously mentioned, this trend in lateral stress in the soil mass corresponded with the tendency of lateral loads on piles in the 5th-row to increase as well.

Fig. 17 illustrates that the arching effect impacts the lateral load capacity of the piles. This effect became more pronounced with increasing vertical load. Consequently, the lateral load capacity of the piled raft was enhanced. When each row of piles was analyzed, it was observed that the front of the 1st-row piles experienced the most pronounced arching effect, while the front of the 5th-row piles exhibited the least arching effect. This phenomenon resulted in a higher lateral load capacity of the 1st-row piles compared to those in the 5th-row, as depicted in Fig. 16. The relationship between lateral load, vertical load, and lateral displacement of piles in rows 1 and 5 exhibited similarities for both PR_OG and PR_EM. Specifically, the lateral load of PR_EM was approximately 20 percent higher than that of PR_OG for piles in the first row, whereas the values for piles in row 5 were roughly similar, especially when considering a lateral displacement of 10 percent of the pile diameter.

4.5 Lateral load sharing of piled raft by the various vertical loads

Fig. 18 shows the relationship between lateral load sharing and displacement of pile and raft while varying the vertical loads on PR_OG and PR_EM. The lateral load share of the raft experienced a notable reduction between 0% and 7% lateral displacements, with a slight further reduction observed beyond 7% displacement. Conversely, the proportion of lateral load shared by the piles exhibited a significant increase within displacements ranging from 0 to 7%, with a slight additional increase noted beyond 7% displacement. Regarding the influence of vertical load on the piled raft, the lateral load share of the raft increased with the vertical load, while the piles received a comparatively lesser share. The lateral load sharing behaviors of PR_OG and PR_EM appeared consistent, with the raft of PR_EM demonstrating a higher lateral load sharing capability than PR_OG, attributed to the former raft being embedded in the soil.

The data revealed that at 7% lateral displacement, the lateral load share of the raft ranged from 10% to 18% for PR_OG and from 27% to 32% for PR_EM. When lateral displacement is beyond 7%, the lateral load share of the raft in both PR_OG and PR_EM experienced a slight decrease. These findings underscore the significant influences of raft embedding and vertical load on the piled raft, particularly in terms of the lateral load-sharing efficiency of PR_EM, which was approximately 15% higher than that of PR_OG.

5. Conclusions

This study aims to investigate the behavior of piled raft foundations under combined vertical and lateral loads, as well as different raft positions, using the finite element method (FEM). The key findings from the numerical analyses are as follows:

- The vertical load sharing of the raft decreases significantly as the vertical load increases up to a certain point (NVL≥40), where it becomes constant. Embedded rafts (PR_EM) demonstrate greater vertical load capacity compared to those placed on top of the ground (PR_OG).
- The rotation angle of piled rafts under vertical and lateral loads increases with lateral displacement and vertical load. PR_EM exhibits lower rotation angles compared to PR_OG due to its embedded position, contributing to stability by distributing lateral loads to the soil.
- Adequate vertical loads (NVL≥40) prevent tensile forces in the piles during lateral loading, irrespective of the raft position.

- The lateral load-carrying capacity of piled rafts increases with vertical load. PR_EM demonstrates higher capacity than PR_OG due to its embedded position.
- Piles in each row show comparable lateral load capacity for lateral displacements up to 3% of the pile diameter, unaffected by vertical load.
- The piled raft's lateral load capacity shows a linear relationship with displacement (<3% of pile diameter), exhibiting elastic behavior.
- The lateral load sharing of the raft decreases significantly with lateral displacement (<7% of pile diameter), further decreasing beyond 7%. PR_EM exhibits larger lateral load sharing due to its embedded position.
- Design considerations should account for lateral loads causing displacement within 3% of the pile diameter to maintain elastic behavior and safety.

In conclusion, this research enhances understanding of piled raft behavior under combined loads and offers insights for design considerations to ensure structural integrity and safety.

Acknowledgments

The authors gratefully acknowledge the financial support from the Faculty of Graduate School, Prince of Songkla University, through the Talent Utilization Type 1 Grant No. TU1-04/2564, Prince of Songkla University (ENG6601098S) and the National Research Council of Thailand and innovation fund and the university of Phayao (no. 231/2567). The authors would like to express sincere gratitude to Prince of Songkla University and Southern Natural Disaster Research Center for providing us with great support and resources in completing this study. We are grateful for their generous funding enabling us to conduct our investigation and complete this research. Furthermore, we extend our deepest thanks to the anonymous reviewers for their meticulous efforts and insightful suggestions, which have significantly enhanced the quality of this paper.

References

Adeel, M.B., Aaqib, M., Pervaiz, U., Rehman, J.U. and Park, D. (2022), "Numerical response of pile foundations in granular soils subjected to lateral load", *Geomech. Eng.*, **28**(1), 11-23. https://doi.org/10.12989/gae.2022.28.1.011.

Amornfa, K., Quang, H.T. and Tuan, T. (2022), "3D numerical analysis of piled raft foundation for Ho Chi Minh City subsoil conditions", *Geomech. Eng.*, **29**(2), 183-192. https://doi.org/10.12989/gae.2022.29.2.183.

Azizkandi, A.S., Baziar, M.H. and Yeznabad, A.F. (2018), "3D dynamic finite element analyses and 1 g shaking table tests on seismic performance of connected and nonconnected piled raft foundations", *KSCE J. Civil Eng.*, **22**(5), 1750-1762. https://doi.org/10.1007/s12205-017-0379-2.

Balakumar, V., Huang, M., Oh, E. and Balasubramaniam, A.S. (2017), "A critical and comparative study on 2D and 3D analyses of raft and piled raft foundations", *Proceedings of the SEAGS 50th Anniversary Symposium*, AIT, Bangkok, Thailand.

Chanda, D., Saha, R., Haldar, S., Nayak, B.C. and Kumar, E.V. (2022), "Scaled modeled tests and finite element numerical study on lateral responses of PRF system under VHM loading", *Geomech. Geoeng.*, 1-25. https://doi.org/10.1080/17486025.2022.2048092.

D'Aguiar, S., Modaressi-Farahmand-Razavi, A., Lopez-Caballero, F. and Santos, J. (2008), "Soil-structure interface modeling: Application to pile axial loading", *Proceedings of the 12th International Conference of the International Association for Computer Methods and Advances in Geomechanics (IACMAG)*, Goa, India.

Halder, P., Manna, B. and Sur, A. (2020), "Impact of pile head rigidity on the response of piled raft in sand under pseudo-static loading", *Indian Geotech. J.*, **50**(5), 810-824. https://doi.org/10.1007/s40098-020-00408-4.

Haouari, H. and Bouafia, A. (2023), "Single piles under monotonic lateral loads-Full scale tests and numerical modelling", *J. Geomech. Geoeng.*, **1**(1), 11-25. https://doi.org/10.38208/jgg.v1i1.441.

Hsueh, C.K., Lin, S.S. and Ong, D.E. (2018), "Finite element analysis to characterize the lateral behaviour of a capped pile group", *Geotech. Eng.*, **49**(2), 22-31.

Jamil, I., Ahmad, I., Rehman, A.U., Ahmed, A., Hamza, A. and Ullah, W. (2022), "Response of basement wall in tall buildings foundation under lateral loading", *Frontiers of Structural and Civil Engineering*, 1-9. https://doi.org/10.1007/s11709-022-0885-2.

Karira, H., Kumar, A., Ali, T.H., Mangnejo, D.A. and Mangi, N. (2022a), "A parametric study of settlement and load transfer mechanism of piled raft due to adjacent excavation using 3D finite element analysis", *Geomech. Eng.*, **30**(2), 169-185. https://doi.org/10.12989/gae.2022.30.2.169.

Karira, H., Kumar, A., Ali, T.H., Mangnejo, D.A. and Yaun, L. (2022b), "Numerical investigation of responses of a piled raft to twin excavations: Role of sand density", *Geomech. Eng.*, **31**(1), 53-69. https://doi.org/10.12989/gae.2022.31.1.053.

Katzenbach, R. And Leppla, S. (2015), "Realistic Modelling of Soil-Structure Interaction for High-Rise Buildings", *Procedia Eng.*, **117**, 162-171. https://doi.org/10.1016/j.proeng.2015.08.137.

Khari, M., Dehghanbandaki, A. and Armaghani, D.J. (2021), "Physical modelling of bending moments in single piles under combined loads in layered soil", *Geomech. Eng.*, **25**(5), 373-381. https://doi.org/10.12989/gae.2021.25.5.373.

Knappett, J. and Craig, R.F. (2019), *Craig's Soil Mechanics (8th Ed.)*, CRC press.

Kumar, A., Choudhury, D. and Katzenbach, R. (2016), "Effect of earthquake on combined pile–raft foundation", *Int. J. Geomech.*, **16**(5), 04016013. https://doi.org/10.1061/(ASCE)GM.1943-5622.0000637.

Likitlersuang, S., Chheng, C., Surarak, C. and Balasubramaniam, A. (2018), "Strength and stiffness parameters of Bangkok clays for finite element analysis", *Geotech. Eng. J. SEAGS & AGSSEA*, **49**(2), 150-156.

Likitlersuang, S., Surarak, C., Wanatowski, D., Oh, E. and Balasubramaniam, A. (2013a), "Finite element analysis of a deep excavation: A case study from the Bangkok MRT", *Soils Found.*, **53**(5), 756-773. https://doi.org/10.1016/j.sandf.2013.08.013.

Likitlersuang, S., Teachavorasinskun, S., Surarak, C., Oh, E. and Balasubramaniam, A. (2013b), "Small strain stiffness and stiffness degradation curve of Bangkok clays", *Soils Found.*, **53**(4), 498-509. https://doi.org/10.1016/j.sandf.2013.06.003.

Luo, X., Shi, Y. and Wang, P. (2022), "Three-dimensional stability assessment of slopes with spatially varying undrained shear strength", *Geomech. Eng.*, **31**(4), 375-384.

https://doi.org/10.12989/gae.2022.31.4.375.
Novak, L.J., Reese, L.C. and Wang, S.-T. (2005), "Analysis of pile-raft foundations with 3D finite-element method", *Proceedings of the Structures Congress 2005*, Metropolis and Beyond.
Plaxis (2020), *Material Models Manual (Version Connect Edition V20.04)*, Bentley Systems, Incorporated, PA, USA.
Poorjafar, A., Esmaeili-Falak, M. and Katebi, H. (2021), "Pile-soil interaction determined by laterally loaded fixed head pile group", *Geomech. Eng.*, **26**(1), 13-25. https://doi.org/10.12989/gae.2021.26.1.013.
Qin, H. and Ma, K. (2021), "Dynamic behaviour difference between high-and low-raft forms of piles in earthquakes", *Geotech. Res.*, **8**(3), 85-92. https://doi.org/10.1680/jgere.20.00044.
Shirato, M., Kohno, T. and Nakatani, S. (2009), "Geotechnical criteria for serviceability limit state of horizontally loaded deep foundations", *In Geotechnical Risk and Safety*, 133-140. CRC Press.
Snyder, J.L. (2004), "Full-scale lateral-load tests of a 3x5 pile group in soft clays and silts", Master of Science; Brigham Young University, Provo, UT 84602, USA.
Soomro, M.A., Mangi, N., Memon, A.H. and Mangnejo, D.A. (2022), "Responses of high-rise building resting on piled raft to adjacent tunnel at different depths relative to piles", *Geomech. Eng.*, **29**(1), 25-40. https://doi.org/10.12989/gae.2022.29.1.025.
Surarak, C. (2010), "Geotechnical aspects of the Bangkok MRT blue line project", Ph.D. Dissertation; Griffith University, Australia.
Tomlinson, M. and Woodward, J. (2007), *Pile design and construction practice*, CRC press.
Vakili, K., Barciaga, T., Lavasan, A. and Schanz, T. (2013), "A practical approach to constitutive models for the analysis of geotechnical problems", *Proceedings of the 3rd International Symposium On Computational Geomechanics (ComGeo III)*, at Krakow, Poland.
Vu, A., Pham, D., Nguyen, T. and He, Y. (2014), "3D finite element analysis on behaviour of piled raft foundations", *Appl. Mech. Mater.*, **580-583**, 3-8. https://doi.org/10.4028/www.scientific.net/amm.580-583.3.
Watcharasawe, K., Kitiyodom, P. and Jongpradist, P. (2017), "3-D numerical analysis of consolidation effect on piled raft foundation in Bangkok subsoil condition", *Int. J. Geomate*, **12**(31), 105-111. http://dx.doi.org/10.21660/2017.31.6529.
Yun, J., Han, J. and Kim, D. (2022), "Evaluation of seismic p-y loops of pile-supported structures installed in saturated sand", *Geomech. Eng.*, **30**(6), 579-586. https://doi.org/10.12989/gae.2022.30.6.579.
Zhao, C., Lavasan, A. A., Barciaga, T., Zarev, V., Datcheva, M. and Schanz, T. (2015), "Model validation and calibration via back analysis for mechanized tunnel simulations–The Western Scheldt tunnel case", *Comput. Geotech.*, **69**, 601-614. https://doi.org/10.1016/j.compgeo.2015.07.003.